

201

⁷LiF AND CaF₂:Mn EXPERIMENTAL DATA FOR
EVALUATING TLD ENERGY RESPONSE THEORY

by

Robert Mark Ostmeyer
B.S., Kansas State University, 1979

A MASTER'S THESIS

submitted in partial fulfillment of the
requirements for the degree

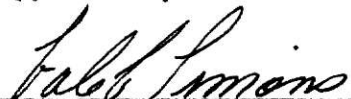
MASTER OF SCIENCE

Department of Nuclear Engineering

KANSAS STATE UNIVERSITY
Manhattan, Kansas

1980

Approved by:


Major Professor

Spec. Coll.
LID
2668
.T4
1980
078
c.2

i

TABLE OF CONTENTS

	<u>Page</u>
LIST OF TABLES	iii
LIST OF FIGURES	v
1.0 INTRODUCTION	1
1.1 History of Method Development and Evaluation.	1
1.2 Scope of Experimentation.	2
2.0 EXPERIMENTAL EQUIPMENT AND MATERIALS	3
2.1 TLD Response Measurement Equipment.	3
2.2 Annealing Equipment	5
2.3 Handling Equipment.	7
2.4 Thermoluminescent Dosimeters.	7
2.5 Encasement Materials.	8
2.6 Gamma Ray Sources	8
2.7 Irradiation Device.	15
3.0 EXPERIMENTAL PROCEDURES.	19
3.1 TLD Handling.	19
3.2 TLD Preannealing.	19
3.3 TLD Calibration	20
3.4 TLD Encapsulation	20
3.5 Exposure/Wait/Response Measurement Schedule	23
3.6 TLD Response Measurement Procedure.	24
3.7 Sensitivity Selection	28
4.0 EXPERIMENTAL RESULTS	35
4.1 TLD Energy Response Results	35
4.2 Sleeve Thickness Effects Results.	41
5.0 THEORETICAL CONSIDERATIONS	55
5.1 The Dose Ratio Factor	55
5.2 The Calculated Dose	55
5.3 Relative Source Counts.	61
5.4 Sleeve Wall Attenuation Considerations.	61
6.0 SLEEVE WALL ATTENUATION OF PRIMARY GAMMAS.	70
6.1 The Effective Attenuation Coefficient	70
6.2 Attenuation Corrected TERC/III Calculations	73
7.0 COMPARISON OF EXPERIMENT AND THEORY.	92
7.1 Calculated and Experimental TLD Doses	92
7.2 Comparison of Attenuation Corrected Doses	97
7.3 The Effective Source Counts Comparison.	97
8.0 CONCLUSIONS.	113

Table of Contents - Continued

	<u>Page</u>
9.0 SUGGESTIONS FOR FURTHER STUDY.	115
REFERENCES.	117
ACKNOWLEDGEMENTS.	119
APPENDIX A: Statistics Equations for Data Reduction.	120
APPENDIX B: TERC/III Input and Output.	125
APPENDIX C: Raw TLD Data	143
APPENDIX D: Ionization Theory	193

**THIS BOOK
CONTAINS
NUMEROUS PAGES
WITH THE ORIGINAL
PRINTING BEING
SKEWED
DIFFERENTLY FROM
THE TOP OF THE
PAGE TO THE
BOTTOM.**

**THIS IS AS RECEIVED
FROM THE
CUSTOMER.**

LIST OF TABLES

<u>Table</u>		<u>Page</u>
2.1	Encasement materials used during measurement of the energy response of encased ^7LiF and $\text{CaF}_2\text{:Mn}$ TLDs.	10
2.2	Encasement materials used during measurement of the wall thickness effect on the energy response of encased ^7LiF and CaF_2 TLDs	11
2.3	Gamma-ray sources purchased for use in the TLD energy response and sleeve thickness studies.	16
3.1	Analyzer settings used for the response measurement of the ^7LiF and $\text{CaF}_2\text{:Mn}$ TLDs	25
4.1	TLD analyzer output normalized to iron encased ^7LiF TLDs from a precision subset	36
4.2	TLD analyzer output normalized to iron encased $\text{CaF}_2\text{:Mn}$ TLDs from a precision subset.	37
4.3	TLD analyzer output normalized to iron encased ^7LiF TLDs corrected for individual sensitivity.	
4.4	TLD analyzer output normalized to iron encased $\text{CaF}_2\text{:Mn}$ TLDs corrected for individual sensitivity	40
5.1	Calculated TLD dose ratios for encased ^7LiF TLDs derived from TERC/III results with iron encased TLDs as the normalizing values.	59
5.2	Calculated TLD dose ratios for encased $\text{CaF}_2\text{:Mn}$ TLDs derived from TERC/III results with iron encased TLDs as the normalizing values.	60
6.1	Effective attenuation coefficients for encased ^7LiF TLDs calculated with sleeve curvature corrections to the sleeves and with TLD readouts corrected for individual sensitivity.	71
6.2	Effective attenuation coefficients for encased $\text{CaF}_2\text{:Mn}$ TLDs calculated with sleeve curvature corrections to the sleeves and with TLD readouts corrected for individual sensitivity.	72
6.3	Calculated TLD dose ratios for encased ^7LiF TLDs derived from attenuation corrected TERC/III results with iron encased TLDs as the normalizing values.	90

List of Tables - Continued

<u>Table</u>		<u>Page</u>
6.4	Calculated TLD dose ratios for encased $\text{CaF}_2\text{:Mn}$ TLDs derived from attenuation corrected TERC/III results with iron encased TLDs as the normalizing values.	91
7.1	Comparison of dose ratios using encapsulated ^7LiF TLDs from a precision subset.	93
7.2	Comparison of dose ratios using encapsulated $\text{CaF}_2\text{:Mn}$ TLDs from a precision subset.	94
7.3	Comparison of dose ratios using encased ^7LiF TLDs where the experimental values were corrected for the sensitivity of individual TLDs.	95
7.4	Comparison of dose ratios using encased $\text{CaF}_2\text{:Mn}$ TLDs where the experimental values were corrected for the sensitivity of individual TLDs.	96
7.5	Comparison of ^7LiF dose ratios where the experimental values were corrected for sensitivity and the calculations were corrected for sleeve wall attenuation. . .	99
7.6	Comparison of $\text{CaF}_2\text{:Mn}$ dose ratios where the experimental values were corrected for sensitivity and the calculations were corrected for sleeve wall attenuation. . .	100

LIST OF FIGURES

<u>Figure</u>		<u>Page</u>
2.1	Photograph of the Harshaw Model 2000 TLD analyzer and CO ₂ gas purge system.	4
2.2	Photograph of the TLD annealing ovens	6
2.3	Photograph depicting the types of thermoluminescent dosimeters used for data acquisition.	9
2.4	Photograph of TLD sleeves used during data acquisition	14
2.5	Gamma-ray source capsule for the TLD energy response and sleeve thickness studies.	17
2.6	Device designed for irradiating thermoluminescent dosimeters (TLDs)	18
3.1	Calibration curve for 1x1x6 mm ⁷ LiF thermoluminescent dosimeters irradiated by a nominal 3.2 mC Cs-137 source.	21
3.2	Calibration curve for 1x1x6 mm CaF ₂ :Mn thermoluminescent dosimeters irradiated by a nominal 3.2 mC Cs-137 source	22
3.3	Heating cycle used for the response measurement of the ⁷ LiF TLDs during the TLD energy response study. . .	26
3.4	Heating cycle used for the response measurement of the CaF ₂ :Mn TLDs during the TLD energy response study .	27
3.5	Heating cycle used for the response measurement of the ⁷ LiF TLDs during the sleeve thickness effects study	30
3.6	Heating cycle used for the response measurement of the CaF ₂ :Mn TLDs during the sleeve thickness effects study	31
3.7	Typical glow curve for ⁷ LiF TLDs with the TLD temperature corresponding to the maximum response rate indicated.	32
3.8	Typical glow curve for the CaF ₂ :Mn TLDs with the TLD temperature corresponding to the maximum response rate indicated.	33

List of Figures - Continued

<u>Figure</u>		<u>Page</u>
3.9	Typical sensitivity data measured for ^7LiF TLDs exposed to a 3.2 mCi Cs-137 gamma-ray source.	34
4.1	Sleeve thickness data obtained by exposing encased ^7LiF TLDs to the Co-57 source	43
4.2	Sleeve thickness data obtained by exposing encased ^7LiF TLDs to the Ce-141 source.	44
4.3	Sleeve thickness data obtained by exposing encased ^7LiF TLDs to the Hg-203 source.	45
4.4	Sleeve thickness data obtained by exposing encased ^7LiF TLDs to the Sn-113 source.	46
4.5	Sleeve thickness data obtained by exposing encased ^7LiF TLDs to the Cs-137 source.	47
4.6	Sleeve thickness data obtained by exposing encased ^7LiF TLDs to the Co-60 source	48
4.7	Sleeve thickness data obtained by exposing encased $\text{CaF}_2\text{:Mn}$ TLDs to the Co-57 source.	49
4.8	Sleeve thickness data obtained by exposing encased $\text{CaF}_2\text{:Mn}$ TLDs to the Ce-141 source	50
4.9	Sleeve thickness data obtained by exposing encased $\text{CaF}_2\text{:Mn}$ TLDs to the Hg-203 source	51
4.10	Sleeve thickness data obtained by exposing encased $\text{CaF}_2\text{:Mn}$ TLDs to the Sn-113 source	52
4.11	Sleeve thickness data obtained by exposing encased $\text{CaF}_2\text{:Mn}$ TLDs to the Cs-137 source	53
4.12	Sleeve thickness data obtained by exposing encased $\text{CaF}_2\text{:Mn}$ TLDs to the Co-60 source.	54
5.1	Variation of $f(T_k)$ as a function of gamma-ray energy and encasement material for ^7LiF	56
5.2	Variation of $f(T_k)$ as a function of gamma-ray energy and encasement material for $\text{CaF}_2\text{:Mn}$	57
5.3	Katz and Penfold empirical range-energy relationship for electrons absorbed in a medium.	63

List of Figures - Continued

<u>Figure</u>		<u>Page</u>
5.4	Illustration of the TLD sleeve in relation to the gamma-ray beam.	66
5.5	Percent curvature correction to the encasing sleeve walls (as a function of cavity radius (r), and radial wall thickness (x/ ρ))	68
6.1	Comparison of the experimentally determined effective attenuation coefficients for lead encased ^7LiF and $\text{CaF}_2\text{:Mn}$ TLDs to the total attenuation and mass energy absorption coefficients for lead.	75
6.2	Comparison of the experimentally determined effective attenuation coefficients for tantalum encased ^7LiF and $\text{CaF}_2\text{:Mn}$ TLDs to the total attenuation and mass energy absorption coefficients for tantalum.	76
6.3	Comparison of the experimentally determined effective attenuation coefficients for tin encased ^7LiF and $\text{CaF}_2\text{:Mn}$ TLDs to the total attenuation and mass energy absorption coefficients for tin.	77
6.4	Comparison of the experimentally determined effective attenuation coefficients for zirconium encased ^7LiF and $\text{CaF}_2\text{:Mn}$ TLDs to the total attenuation and mass energy absorption coefficients for zirconium.	78
6.5	Comparison of the experimentally determined effective attenuation coefficients for copper encased ^7LiF and $\text{CaF}_2\text{:Mn}$ TLDs to the total attenuation and mass energy absorption coefficients for copper.	79
6.6	Comparison of the experimentally determined effective attenuation coefficients for iron encased ^7LiF and $\text{CaF}_2\text{:Mn}$ TLDs to the total attenuation and mass energy absorption coefficients for iron.	80
6.7	Comparison of the experimentally determined effective attenuation coefficients for stainless steel encased ^7LiF and $\text{CaF}_2\text{:Mn}$ TLDs to the total attenuation and mass energy absorption coefficients for stainless steel	81
6.8	Comparison of the experimentally determined effective attenuation coefficients for aluminum encased ^7LiF and $\text{CaF}_2\text{:Mn}$ TLDs to the total attenuation and mass energy absorption coefficients for aluminum	82

List of Figures - Continued

<u>Figure</u>		<u>Page</u>
6.9	Comparison of the experimentally determined effective attenuation coefficients for LiF encased ⁷ LiF and CaF ₂ :Mn TLDs to the total attenuation and mass energy absorption coefficients for LiF.	83
6.10	Illustration of the attenuation correction to the dose ratio for ⁷ LiF TLDs encased in 0.7 g/cm ² Pb, Zr and stainless steel.	84
6.11	Illustration of the attenuation correction to the dose ratio for ⁷ LiF TLDs encased in 0.7 g/cm ² Ta, Cu, and Al sleeves	85
6.12	Illustration of the attenuation correction to the dose ratio for ⁷ LiF TLDs encased in 0.7 g/cm ² Sn, Cu, and LiF sleeves.	86
6.13	Illustration of the attenuation correction to the dose ratio for CaF ₂ :Mn TLDs encased in 0.7 g/cm ² Pb, Zr, and stainless steel sleeves.	87
6.14	Illustration of the attenuation correction to the dose ratio for CaF ₂ :Mn TLDs encased in 0.7 g/cm ² Ta, Cu, and Al sleeves	88
6.15	Illustration of the attenuation correction to the dose ratio for CaF ₂ :Mn TLDs encased in 0.7 g/cm ² Sn, Fe, and LiF sleeves.	89
7.1	Relative number of source decays from Co-60 irradiated encased ⁷ LiF TLDs as a function of encasement material atomic number	101
7.2	Relative number of source decays from Cs-137 irradiated encased ⁷ LiF TLDs as a function of encasement material atomic number	102
7.3	Relative number of source decays from Sn-113 irradiated encased ⁷ LiF TLDs as a function of encasement material atomic number.	103
7.4	Relative number of source decays from Hg-203 irradiated encased ⁷ LiF TLDs as a function of encasement material atomic number	104
7.5	Relative number of source decays from Ce-141 irradiated encased ⁷ LiF TLDs as a function of encasement material atomic number.	105

List of Figures - Continued

<u>Figure</u>		<u>Page</u>
7.6	Relative number of source decays from Co-57 irradiated encased LiF TLDs as a function of encasement material atomic number.	106
7.7	Relative number of source decays from Co-60 irradiated encased $\text{CaF}_2\text{:Mn}$ TLDs as a function of encasement material atomic number.	107
7.8	Relative number of source decays from Cs-137 irradiated encased $\text{CaF}_2\text{:Mn}$ TLDs as a function of encasement material atomic number.	108
7.9	Relative number of source decays from Sn-113 irradiated encased $\text{CaF}_2\text{:Mn}$ TLDs as a function of encasement material atomic number.	109
7.10	Relative number of source decays from Hg-203 irradiated encased $\text{CaF}_2\text{:Mn}$ TLDs as a function of encasement material atomic number.	110
7.11	Relative number of source decays from Ce-141 irradiated encased $\text{CaF}_2\text{:Mn}$ TLDs as a function of encasement material atomic number.	111
7.12	Relative number of source decays from Co-57 irradiated encased $\text{CaF}_2\text{:Mn}$ TLDs as a function of encasement material atomic number.	112

1.0. INTRODUCTION

During the past decade, thermoluminescent dosimeters (TLDs) have received international attention for the measurement of gamma energy deposition, in various regions of low power critical assemblies. This interest was largely generated by the successful demonstration of the method by scientists within Argonne National Laboratory's Applied Physics Division^{1,2,3}. Specific measurements for which this method has been employed include (1) characterizations of fast reactor assemblies^{1,4-6}, (2) energy deposition in shielding materials^{7,8}, (3) gamma heating measurements in fast breeder reactor blankets⁹, and (4) energy deposition in reactor control rods^{10,11}.

1.1 History of Method Development and Evaluation

The particular advantage of using TLDs for gamma heating measurements, is the small size of the dosimeters. When placed within a gamma irradiated medium, the TLDs do not appreciably perturb the gamma field. This non-perturbation characteristic is desirable when a good estimate of the surrounding medium's radiation dose is required. Nevertheless, despite their small size, TLDs exhibit a linear response as a function of gamma dose over a wide range of radiation exposures¹². However, it should be mentioned that this linear response characteristic holds only when the radiation makeup remains unchanged.

The theory used to relate absorption of gamma radiation in a medium, to that of the resulting ionization produced in a TLD, was forwarded by T.E. Burlin^{13,14}. Based upon this theory, various com-

putational methods were developed to determine this relationship^{15,16}. One such method is incorporated into the TERC/III computer code, which was developed by scientists at Argonne National Laboratory.

Once the computational methods were developed, raw TLD data were acquired for their evaluation^{17,18}. This was accomplished by gamma irradiation of encased ^7LiF TLDs. The encasements included sleeves of B_4C , Teflon, iron, copper, lead, stainless steel, tantalum, and aluminum. The studied gamma energies ranged from 0.662 to 1.333 MeV. With comparison of the experimental results to the computational methods, good correlation was found to exist.

1.2 Scope of Experimentation

In order to further evaluate the various computational methods, a broader data base needed to be generated. As a result of this need, response data were obtained by irradiating encased ^7LiF and $\text{CaF}_2:\text{Mn}$ TLDs. Encasements included sleeves made of lead, tantalum, tin, zirconium, copper, stainless steel, iron, aluminum and natural LiF . Gamma energies ranged from 0.122 to 1.333 MeV. The experimentally determined energy response results, and comparisons between these results and TERC/III calculations, are presented.

To compliment the energy response study, the results of a sleeve thickness investigation are also reported. For this study, ^7LiF and $\text{CaF}_2:\text{Mn}$ response data were obtained using a variety of sleeve thicknesses. The investigated gamma energies and sleeve materials were the same as those used for the TLD energy response study.

2.0 EXPERIMENTAL EQUIPMENT AND MATERIALS

Equipment and materials, which were available for the performance of the experimental phase of these investigations, are described in this chapter. Except for the TLD encasing materials, which were on loan from Argonne National Laboratory, all items were purchased with available research funds.

2.1 TLD Response Measurement Equipment

During execution of the TLD energy response study, individual dosimeter responses were measured using a Harshaw 2000 TLD Reader. A photograph of the equipment is shown in Fig. 2.1. This particular analyzer consisted of two major components, a 2000-A Thermoluminescence (TL) Detector and a 2000-B Automatic Integrating Picoammeter. A CO₂ gas metering system was connected to the 2000-A unit for the purpose of purging the TLD heating chamber of residual air. In the course of normal operation, the TL detector utilized a photomultiplier tube (PMT) to measure the individual TL emissions released during prescribed TLD heating cycles. During measurement of these heat induced emissions, the PMT currents were simultaneously integrated by the 2000-B unit. These integrations produced LED readings of total charge, which were relative measures of total TLD response. This was the desired quantity used to relate the instrument output to the gamma-ray induced excitation within the dosimeters.

To complete the sleeve-thickness study, individual TLD responses were measured with two analyzers, namely the Harshaw 2000, and a photon

**THIS BOOK
CONTAINS
NUMEROUS PAGES
WITH PICTURES
THAT ARE CROOKED
COMPARED TO THE
REST OF THE
INFORMATION ON
THE PAGE.**

**THIS IS AS RECEIVED
FROM CUSTOMER.**

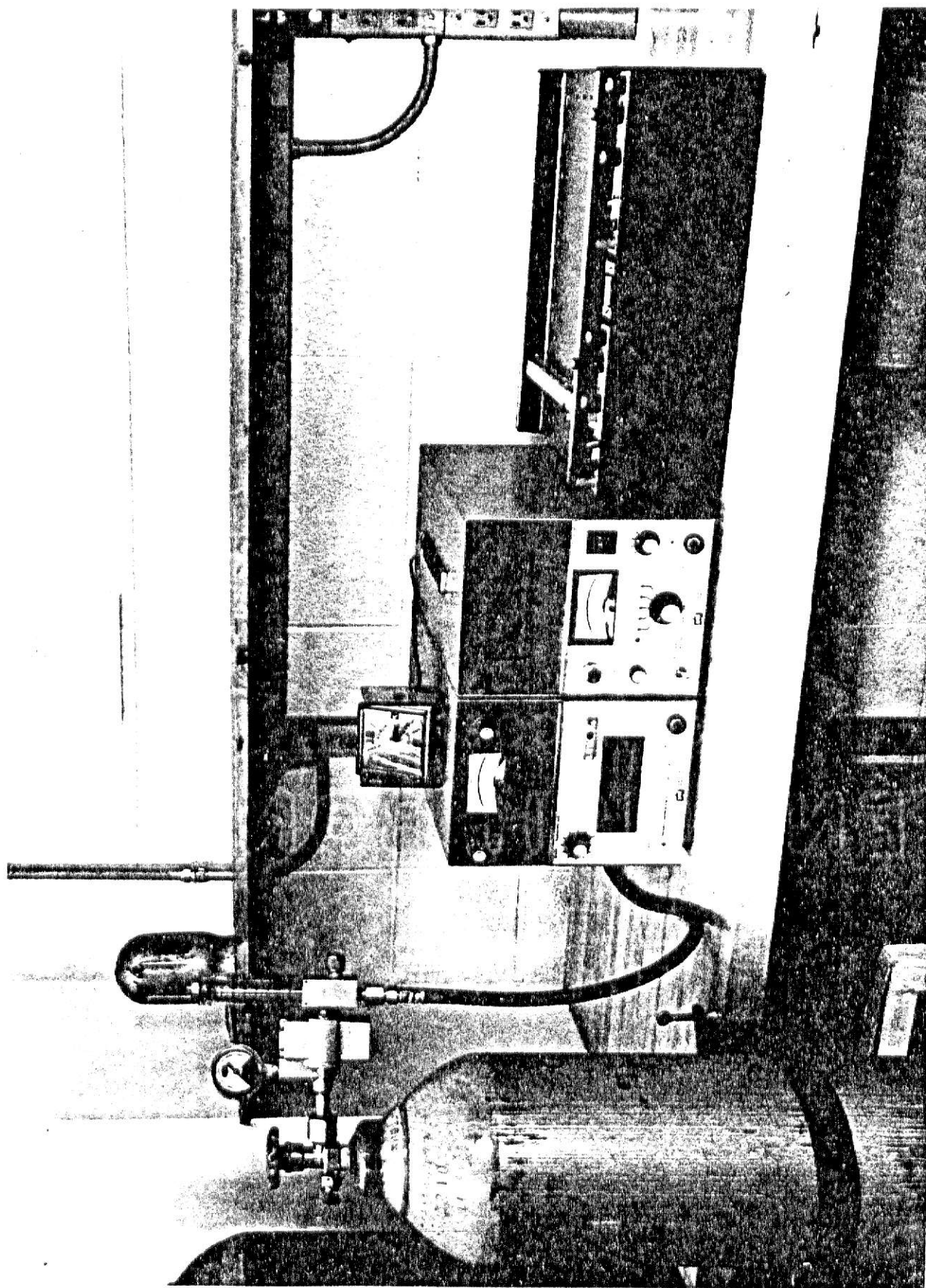


Fig. 2.1. Photograph of the Harshaw Model 2000 TLD analyzer and CO₂ gas purge system.

detection system which was developed within the Nuclear Engineering Department at Kansas State University. A detailed discussion of the photon analyzer's operating characteristics is presented in Ref. 19. Basically, the photon detecting system differs from the Harshaw analyzer in only two respects. First, the total number of photons detected by the PMT (rather than the PMT current) is integrated and second, N_2 (rather than CO_2) gas is used for purging of the TLD heating chamber. In a manner similar to the integrated charge result for the Harshaw 2000, the integrated number of photon counts is the quantity used to relate instrument output to the radiation induced excitation within the TLDs.

An X-Y recorder was employed in concurrence with both analyzers during data acquisition. It was used to generate glow curves (PMT response rate versus time) and temperature profiles whenever permanent records were required. Normally, only the integrated responses were recorded.

2.2 Annealing Equipment

Two ovens (see Fig. 2.2) and a draft-free drawer were available for annealing of TLDs prior to radiation exposures. The first oven, a Thermolyne Type 10500 furnace with solid state temperature control, and an operating range of 30-1200°C, was used for TLD annealing at 400°C. A Thelco Model 16 Precision Oven, with an operating range of 0-200°C, was employed for TLD annealing at 100°C.

Pyrex petri dishes were used as TLD receptacles during the pre-annealing procedure. Pyrex glass was chosen because its surface is

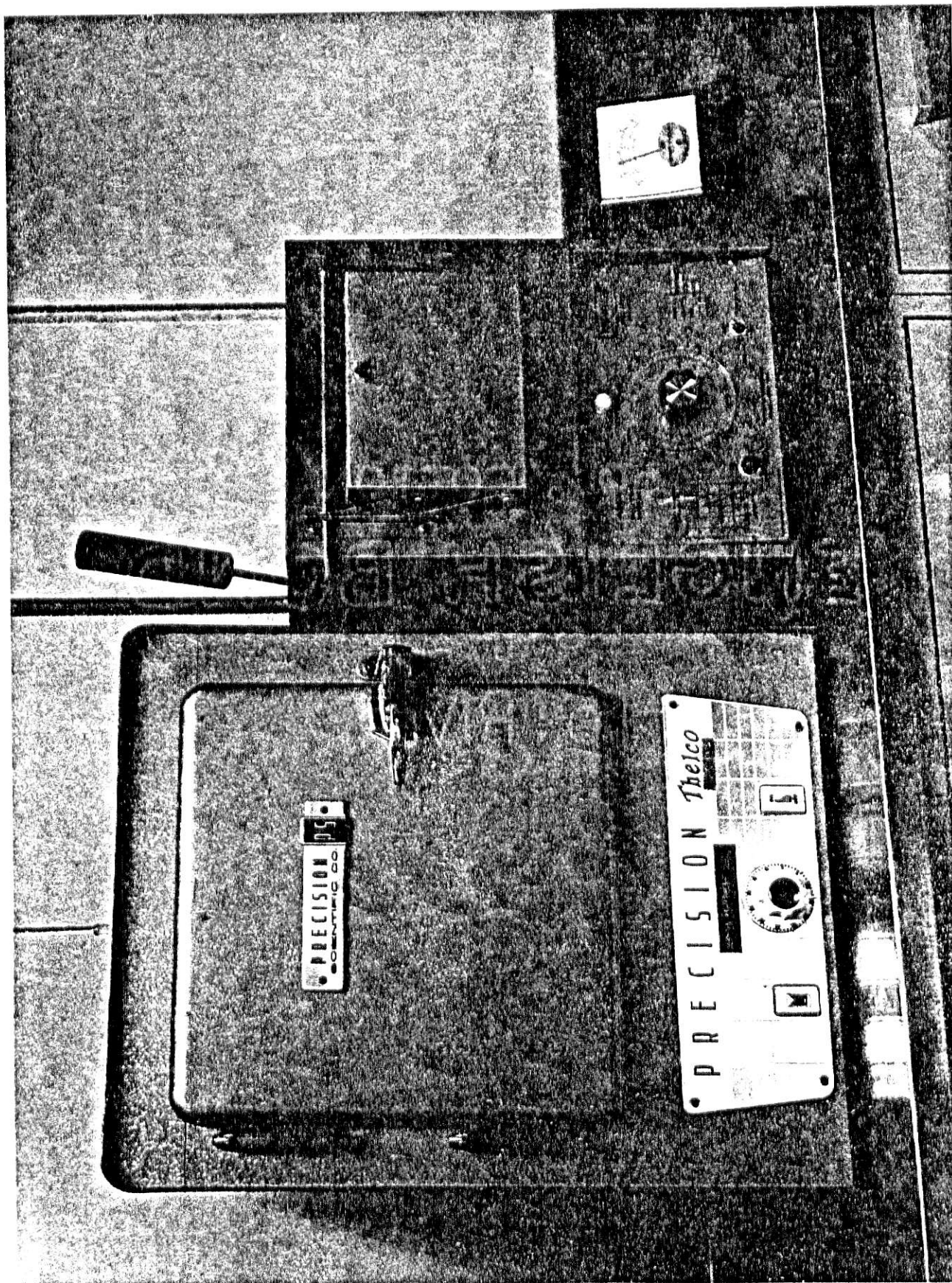


Fig. 2.2. Photograph of the TLD annealing ovens.

resistant to oxidation at high temperatures. If a material not resistant to this formation was chosen, the surfaces of the TLDs could have been contaminated. This occurrence would have had a detrimental affect on the precision of the dosimeters.

A draft free drawer, located directly below the ovens, was used for cooling the TLD laden petri dishes. Situated at the bottom of the drawer was a sheet of asbestos upon which the receptacles were placed. The asbestos pad was used to avoid any appreciable drawer-bottom conduction cooling of the dishes. Prevention of this phenomenon allowed for slower and more reproducible TLD cooling rates. Rapid cooling tends to increase the size of the undesirable low temperature TLD response peaks¹².

2.3 Handling Equipment

TLDs were handled using a special plastic tipped tweezers. The tweezers was used to avoid abrasion or crushing of the delicate dosimeters. If incurred, both of these phenomena could have affected a TLD's response characteristics.

In order to maintain the individuality of each TLD, the dosimeters were stored in numbered coin envelopes. The envelopes were chosen because of their amenability to storage and cataloging.

2.4 Thermoluminescent Dosimeters

One thousand new TLDs of two varieties were purchased for the energy response study. The first type consisted of Harshaw TL-700 (^7LiF) 1x1x6 mm rods enriched to 99.993 percent ^7Li . The second consisted of

Harshaw TL-400 ($\text{CaF}_2\text{:Mn}$) rods of the same size. A closeup photograph of the two varieties is shown in Fig. 2.3.

2.5 Encasement Materials

The set of encasement materials (sleeves) employed for the TLD energy response study consisted of ten encasements each of the materials lead, tantalum, tin, zirconium, copper, iron, stainless steel, aluminum, and natural LiF. All sleeves were cylindrical in shape and approximately one-half inch in length. For each encasement, the radial wall mass thickness was nominally 0.7 g/cm^2 . The number of sleeves available and their associated physical parameters are presented in Table 2.1.

For the sleeve thickness investigation, the encasements consisted of the same variety of materials discussed above (see Table 2.2). As may be observed, there were a number of different radial wall thicknesses for each encasement material. Also, indicated for each wall thickness is a wall-curvature correction ratio with the associated corrected wall thickness. These corrected thicknesses were calculated to compensate for wall curvature since the encased dosimeters were irradiated using essentially a monodirectional gamma flux. This correction is discussed in much greater detail in Section 5.3. All the sleeves employed during both investigations are shown in Fig. 2.4.

2.6 Gamma Ray Sources

Six sources, purchased from Isotope Products Laboratory, were used for the energy response and sleeve thickness investigations. A com-